Solid State Ionics 323 (2018) 37–43

Contents lists available at ScienceDirect

Solid State Ionics

journal homepage: www.elsevier.com/locate/ssi

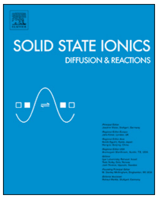

Effect of isovalent doping on grain boundary conductivity for $La_2Mo_2O_9$ oxide ion conductor: A distribution function of relaxation times approach

Tanmoy Paul*, Yoed Tsur

Department of Chemical Engineering and the Grand Technion Energy Program, Technion-Israel Institute of Technology, Haifa 3200003, Israel

ARTICLE INFO

Keywords:
Oxide ion conductor
Impedance spectroscopy
Grain boundary
Space charge

ABSTRACT

In this work we have studied the effect of grain boundary space charge on oxide ion conductivity of $La_{2-x}Er_xMo_2O_9$ ($0.05 \le x \le 0.25$) ionic conductors. Microstructure is studied by scanning electron microscopy and high resolution transmission electron microscopy. Impedance spectra are analyzed in the frame work of impedance spectroscopy genetic programming method. A distribution function of relaxation times model is obtained, which is comprised of two peaks and correlated with the contribution from grain and grain boundary conductivities. The activation energies obtained for both grain and grain boundary conductivities confirm thermally activated hopping of oxygen. Theoretical analysis is carried out to estimate the grain boundary space charge potential at different temperatures for all compositions. The depletion of oxygen vacancies in the space charge layer is also determined. Despite the fact that Er is an isovalent dopant, both the space charge potential and oxygen vacancies are found to be composition dependent. The increase in space charge potential is related to decrease in grain boundary conductivity.

1. Introduction

Fast oxide ion conductors draw a lot of interest due to their potential applications in solid oxide fuel cells, oxygen gas sensors, oxygen pumps and oxygen gas separation membranes. Yttria stabilized zirconia (YSZ), doped $LaGaO_3$ type perovskite, doped ceria and $La_2Mo_2O_9$ have been proved to be successful for electrochemical uses [1–4]. It has been observed that $La_2Mo_2O_9$ shows comparable conductivity with that of YSZ at 1073 K [4]. $La_2Mo_2O_9$ undergoes a structural phase transition from room temperature monoclinic (α phase) to high temperature cubic (β phase) at 853 K with a conductivity enhancement of up to two orders of magnitude [4,5]. Thus it was of utmost interest to find avenues to stabilize the cubic phase down to lower temperatures by doping [6–11]. Here we study how a doping affects the microstructure and electrical properties of the materials.

Different preparation techniques have been used to enhance oxide ion conductivity as well as to produce highly dense samples with uniform particle size for both undoped and doped $La_2Mo_2O_9$ compounds [4,12–21]. In $La_2Mo_2O_9$ prepared by solid state reaction method and sintered at 1173 K without ball-milling of the cationic mixtures, both the grain and grain boundary have conductivities at the same order of magnitude [12]. On the other hand, $La_2Mo_2O_9$ prepared by solid state reaction method at 1323 K with ball-milling of the cationic mixtures has higher grain boundary conductivity as compared to the bulk [13]. Overall, the preparation technique has an effect on conductivity.

Technically the grain boundary resistivity is very much influenced by the sintering temperature of the pellets, the grain size and the dopant concentration. To the best of our knowledge, there is no report on this system explaining the composition dependence of ionic conductivity with special emphasis on grain boundary resistivity. As an intrinsic property, the grain boundaries block the ionic transport across them inferring the grain boundary blocking effect [22–25]. Although there is a channeling of oxygen vacancy across the grain boundary [26]. This grain boundary blocking effect regarding the ionic transport, is mainly attributed to grain boundary core and space charge layers associated with it. The knowledge on space charge layers adjacent to the grain boundary core is also lacking for such system. The space charge layer stretches along a few Debye lengths and suppresses the ionic conductivity by orders of magnitude [27,28]. In general, the layer has a parabolic decay of the charge carrier concentration in logarithmic length scale at the vicinity of the grain boundary core [29].

Impedance data can aid in determining the grain boundary thickness which is an important parameter to analyze the grain boundary conductivity [29–34]. However, the widely used equivalent circuit analysis has a number of known problems such as non-uniqueness. Here we use impedance spectroscopy genetic programming (ISGP), an analysis technique employing evolutionary programming, to find a suitable distribution function of relaxation times (DFRTs) [35,36]. The program

---

* Corresponding author.
E-mail address: paultanmoy00@gmail.com (T. Paul).

https://doi.org/10.1016/j.ssi.2018.05.011
Received 30 October 2017; Received in revised form 4 May 2018; Accepted 13 May 2018

is attractive for better understanding of the physical processes taking place in various electrochemical devices, such as solid oxide fuel cells, solid oxygen electrolysis cells and supercapacitors [37–41].

In this paper we present ac impedance measurements on Er doped $La_2Mo_2O_9$ compounds prepared by solid state reaction at fixed sintering temperature with an emphasis on the space charge layer at the grain boundaries. ISGP is employed to analyze the grain boundary conductivity precisely. The grain and grain boundary conductivities are identified and then distinguished in the DFRT. The grain boundary space charge potential is determined using theoretical consideration [42,43]. The concentration of oxygen vacancies in the space charge layer is also estimated.

2. Experimental and analysis method

Samples of compositions $La_{2-x}Er_xMo_2O_9$ ($0.05 \le x \le 0.25$) were prepared by solid state reaction method. Appropriate amounts of La_2O_3 (sigma Aldrich, 99.9%), MoO_3 (sigma Aldrich, ≥99.5%, with main impurities of Pb ≤ 0.005%, SiO_2 ≤ 0.001% and sulphate ≤ 0.02%) and $Er(NO_3)_3{\cdot}5H_2O$ (sigma Aldrich, 99.9%) were mixed properly in ethanol. Then the dried mixtures were heated in alumina crucible in a chamber furnace at 773 K for 12 h. After cooling, the calcined mixtures were pressed into pellets of 1 mm thick and 13 mm diameter and then sintered at 1223 K for 12 h in air. After sintering, the samples were confirmed by X-ray diffraction to have cubic phase as obtained from the supporting information (Fig. S1). Cubic phase stabilization occurs when doping with ions having similar ionic radii, between La^{3+} and Er^{3+} [20]. The microstructures were also analyzed using scanning electron microscope (Zeiss, Ultra-Plus) and a 200 kV Schottky field emission microscope (JEOL JEM, 2100F). Energy dispersive X-ray (EDX) spectrum was obtained with 10 kV tension line at 6.5 mm working distance coupled with SEM study. Silver was painted on the surfaces of the pellets and thereafter dried for 30 min at 423 K. Impedance spectroscopy was performed from 478 K to 748 K in air in the frequency range of 10 Hz to 2 MHz with 100 mV ac amplitude and without bias, using an impedance analyzer (Biologic, Model VSP) after temperature stabilization of 30 min.

The impedance spectra were analyzed using ISGP to obtain DFRTs. To identify the physical phenomena that are correlated with each peak in the DFRT, several runs with change in one parameter at a time were performed. The results are a shift in the DFRTs peaks with variation in area. At low frequency we obtained a spike-like extension, except for x = 0.25 (see Fig. 1). Such spike contributes an out of range peak in DFRT as described in the next section. To remove the effect of the spike and to find more accurate information from the semicircular arc only, we analyzed the data by a two-iteration process. At first the analysis was done with the spike, letting ISGP seek an out of range peak as a part of the DFRT. Then the contribution of the spike-related out of range peak was subtracted from the total response. After that, a second run of ISGP has been done with the corrected data. Each run is repeated automatically three times at the same initial conditions in order to ensure that the result is not a local minimum.

3. Results and discussion

The normalized impedance plots at 578 K for all compositions and the corresponding fits to the DFRT models are presented in Fig. 1. It is observed that up to x = 0.20, Fig. 1(a), (b), (c) and (d), the response consists of one broad single arc with a spike at low frequencies, whereas two distinguished arcs are observed at x = 0.25, Fig. 1(e). In Fig. 1(f) and its inset, the normalized impedance arcs are shown before and after subtraction for x = 0.15 at 678 K with respective ISGP fitting. The DFRTs (Γ vs. log τ) for $0.05 \le x \le 0.20$ consist of three peaks before subtraction (their exact functional shape has no specific physical meaning and could be any of the following: Gaussian, pseudo-delta, Lorentzian or hyperbolic Secant, see Fig. 2(a) for example). However, we consider two peaks only, as the third peak, in the low frequency region, are out of the frequency range. The DFRT is also shown in Fig. 2(b) after using the subtraction as described in the experimental section. Additionally, the DFRTs as chosen by the program within the measured frequency range for x = 0.25 are shown in Fig. 2(c). We have not used the subtraction technique for x = 0.25 as none of the central peak positions in the DFRTs are out of the measuring range. At all studied temperatures those, DFRTs show two peaks (P1 and P2). The area of each peak is calculated separately and is multiplied by the maximum (un-normalized) resistivity to find the corresponding resistance (R). In general $RC_{eff} = \tau_0$, where C_{eff} is the reactance/capacitance and τ_0 the central peak position. Since the program output consists both a model and fitting of its parameters to match the experimental data, the consistency of the model is examined by the program. Each chosen model is a combination of different standard functional shapes as stated earlier. Having the best possible model in terms of accuracy while using minimal number of free parameters are ensured by a discrepancy-complexity plot [44]. A typical discrepancy-complexity plot is shown for x = 0.25 in Fig. 2(d) obtained from fitting of Fig. 2(c). The best and chosen model has complexity 6 free parameters.

The values of C_{eff} are of the order of 10^{-11} F and 10^{-9} F for peaks P1 and P2 respectively for x = 0.25. Hence peak P1 can be related to the grains and peak P2 is due to grain boundaries. For other compositions we have obtained similar C_{eff} values for both grain and grain boundary (see Table S1 in the Supplementary information). The reciprocal temperature dependence for the grain (σ_{gi}) and grain boundary conductivities (σ_{gb}) are shown in Figs. 3 and 4 respectively for all the compositions. The grain and grain boundary conductivities are obtained as $\sigma_{gi} = \frac{l}{R_{gi}A}$ and $\sigma_{gb} = \frac{l}{R_{gb}A}$, where l is the thickness of the pellet, A is the area of the electrode, R_{gi} and R_{gb} are grain and grain boundary resistances respectively as found by ISGP. The activation energy for ion conduction is obtained from the following relation

$$\sigma = AT^{-1}\exp\left(-\frac{E_a}{K_BT}\right) \tag{1}$$

where A is a pre-exponential factor, E_a is the activation energy of the associated process, K_B is the Boltzmann constant and T is the absolute temperature. Such behavior of ionic conductivity was recently reported for Bi and Y doped samples as well [16,17]. Presently, we have shown electrical data up to 748 K, as above this temperature the effect of electrode polarization dominates [20]. The solid lines in Figs. 3 and 4 indicate the linear least square fits using Eq. (1) and the values of $E_{a/gi}$ and $E_{a/gb}$ (for grain and grain boundary respectively) are also presented in Table 1. It is observed that the activation energy due to grain boundary conductivity is smaller than that of the grain. The activation energy, ~1 eV, indicates diffusion of oxide ions via vacancies [16,45].

The microstructure of the compounds is characterized by SEM as shown in Fig. 5(a) (for x = 0.20). The grains are isolated by well-defined grain boundaries as obtained from the figure. In this context we have discussed the 'line X-ray acquisition' scan using energy dispersive X-ray spectrum (EDX) to obtain the distribution of elements for both grain and grain boundary for all the compositions (see Figs. S2–S7 in the Supplementary information). We perform a line scan of EDX using 5 points and 20 points depending on the surface of the microstructures. We find at least one point and two points on the grain boundary during this 5 points and 20 points line scans respectively. The EDX spectra confirm the similar nature of peaks containing La, Er, Mo and O for all the compositions both in grain and grain boundaries inferring the validity of the incorporation reaction as described later. The resemblance of experimental EDX spectra with that of the simulated pattern confirms the stoichiometry of the composition (see Fig. S3). Furthermore this analysis also suggests that along the grain boundary there is no secondary phase.

The thickness of the grain boundary obtained from high resolution